INTERNATIONAL JOURNAL FOR NUMERICAL METHODS IN FLUIDS, VOL. 2, 185–207 (1982)

ANALYSIS OF TWO-DIMENSIONAL, FINITE AMPLITUDE WAVE PROPAGATION BY TIME MARCHING METHODS

R. PARKER* AND M. N. JAMES†

Department of Mechanical Engineering, University College of Swansea, Singleton Park, Swansea SA2 8PP, U.K.

SUMMARY

Two-dimensional, finite-amplitude wave propagation in an inviscid, subsonic, perfect gas medium is analysed by explicit finite-difference methods. A two-step, Lax–Wendroff method and the single-step, Lax–Friedrichs method are used. A prescribed propagating velocity or pressure disturbance is applied along a single row of grid points normal to the stream direction and results in a 'forced' outflow boundary. The inflow boundary is placed far from outflow by utilizing a streamwise expanding grid and uniform inflow is imposed. Side boundaries are spatially periodic. The numerical solutions are compared with analytical small-perturbation solutions; higher-order effects arising from non-linearities are revealed by Fourier analysis. Solutions which closely approached a periodic state were obtained. The Lax–Wendroff method combined with the expanding grid is shown to be accurate and stable, the Lax–Friedrichs scheme produced highly damped solutions.

1. INTRODUCTION

The use of time-marching for resolving fluid flows in, for example, axial flow turbomachinery cascades can be broadly divided into two categories:

(i) For time-asymptotic steady solutions. These are the familiar procedures where a set of initial values is chosen and the time-dependent governing equations time-marched, in conjunction with boundary conditions, until a steady flow is attained. The steady flow fields of isolated stators and isolated rotor cascades (using a frame of reference moving with the rotor) are determinable in this manner. However, physical meaning is usually only attached to the final steady state, the numerical results between initiation and convergence being discarded—usually with good justification since devices for accelerating convergence, the use of artificial stabilizers, and incorrect boundary conditions can result in a poor approximation to the unsteady flow regime.

(ii) For unsteady, small-perturbation solutions. These involve linearizing the time-dependent governing equations by assuming that the flow field consists of small amplitude periodic variations superimposed on a known steady flow. The resulting equations are then time-marched until a steady amplitude solution is obtained; the solutions being qualitative in nature and only valid for small amplitudes. Different formulations for subsonic and supersonic flows may be necessary. Ni and Sisto[1] use a formulation which is valid for both Mach number regimes to compute the flow field around a harmonically vibrating, flat plate cascade (pertaining to flutter analysis), where a 'forced' periodic solution is desired.

---

* Reader.

† Senior Research Assistant.

0271–2091/82/020185–23$02.30

Received 17 November 1980

Revised 7 October 1981

Time-marching, which has little restriction on Mach number or amplitude, could, if properly applied, provide quantitative data for design work in areas where trial-and-error, or empiricism currently predominate. Moretti[2] discusses the feasibility of using time-marching for unsteady flows, but as far as the authors are aware, a recent paper by Erdos, Alzner and McNally[3] is the only attempt to apply time-marching to unsteady flows in the fully non-linear case. The computation of the periodic, inviscid, rotor–stator interaction in a transonic fan stage is discussed: it involves using a frame of reference fixed to the rotor in conjuction with a fixed frame for the stator. A co-ordinate transformation from the physical plane to an appropriate computational domain is involved and the resulting procedure loses much of the conceptual simplicity of the time-marching method.

This paper presents the results achieved in the application of time-marching to the propagation of finite amplitude waves through a flow field, without the use of co-ordinate transformation. This retains the conceptual simplicity of the method (and will therefore facilitate use with boundaries of arbitrary shape) but has the disadvantage that the computational field must be limited to a practical size, the treatment of the resulting computational boundaries is emphasized. A simple flow configuration (shown in Figure 1) was used. Initial values consisted of a sinusoidal perturbation (obtained from a small-perturbation solution) superimposed on a uniform, subsonic stream.

Along the outflow boundary one wavelength of a propagating finite-amplitude disturbance was maintained (corresponding to a pressure amplitude of 1/10 of an atmosphere). A prescribed streamwise velocity (or pressure) distribution was used for this purpose and a 'forced' system resulted. The remaining unprescribed variables were updated by upstream finite-difference methods. The frequency of the prescribed variation was chosen so that amplitudes decreased towards inflow (i.e. a spatially decaying system; this is discussed in Appendix I). The side boundaries were made spatially periodic and the region of interest was $\mathscr{R}_1$, thus $x = L_1$ was the effective computational boundary. The objective was to time-march the interior of region $\mathscr{R}_1$, in conjunction with the boundary conditions stated above to a periodic state by using finite-difference schemes based on central-differencing, without influence of wave reflections from the inflow boundary. The region $\mathscr{R}_1$ was always covered with a uniform grid (constant Δx, Δy).

The auxiliary grid in region $\mathscr{R}_2$ was used in two ways.

(i) With a uniform grid forming an extension of $\mathscr{R}_1$, computations were continued until steady periodic conditions were established in $\mathscr{R}_1$, whereas $\mathscr{R}_2$ was sufficiently long to ensure that disturbances (propagating from $\mathscr{R}_1$) had not reached $x = L_e$ (and hence could not be

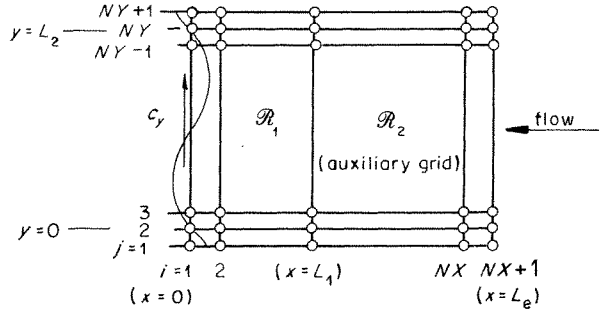

Figure 1. Computation grid for non-linear wave motion

reflected) when the computation was terminated. This facilitated development of a satisfactory treatment of the outflow boundary without influence from the inflow boundary and provided a datum for assessing inflow boundary treatments.

(ii) With an expanding grid to allow a large value of L_e while limiting the number of grid points.

The use of an auxiliary grid incurs computational time and storage which must be minimized in any practical application. A number of simple treatments requiring only one auxiliary row ($L_e = L_1 + \Delta x$) where considered but none were found to be satisfactory, Appendix II.2 presents a list of these with brief explanatory notes.

2. GOVERNING EQUATIONS AND UPDATING SEQUENCE

For compressible flow of a non-conducting, inviscid perfect gas, the governing equations in conservation form are

$$\frac{\partial \mathbf{U}}{\partial t} + \frac{\partial \mathbf{F}(\mathbf{U})}{\partial x} + \frac{\partial \mathbf{G}(\mathbf{U})}{\partial y} = 0 \tag{1}$$

where

$$\mathbf{U} = \begin{bmatrix} \rho \\ m \\ n \\ e_v \end{bmatrix} \qquad \mathbf{F}(\mathbf{U}) = \begin{bmatrix} m \\ p + m^2/\rho \\ mn/\rho \\ m(e_v + p)/\rho \end{bmatrix} \qquad \mathbf{G}(\mathbf{U}) = \begin{bmatrix} n \\ mn/\rho \\ p + n^2/\rho \\ n(e_v + p)/\rho \end{bmatrix} \tag{2}$$

and

$$p = (\gamma - 1)\left[e_v - \frac{m^2 + n^2}{2\rho}\right] \tag{3}$$

i.e. p can be expressed in terms of $\mathbf{U}$. The interior point finite-difference schemes (Section 3) are based on this system of equations; these in turn are used to compute the finite-amplitude (i.e. non-linear) wave propagation discussed in Section 4.

For comparison purposes, setting of initial values and as an aid to formulating boundary conditions, corresponding small-perturbation solutions (valid for small amplitude, and hence linear, wave propagation) are used. These are given in Appendix I.

The updating sequence has five stages (referring to Figure 1 and assuming that $\mathbf{U}$ is known at time level n at all points of the spatial grid (i.e. for $i = 1, \ldots, NX+1$; $j = 1, \ldots, NY+1$)):

(1) The interior points are updated (i.e. $\mathbf{U}_{i,j}^{n+1}$ is obtained for $i = 2, \ldots, NX$; $j = 2, \ldots, NY$).

(2) Points along the $x = 0$ outflow boundary are then updated (i.e. $\mathbf{U}_{i,j}^{n+1}$ is obtained for $i = 1$; $j = 2, \ldots, NY$).

(3) The updated values of streamwise velocity (or pressure) along the outflow boundary are discarded and replaced by a prescribed distribution (which is sinusoidal and of wavelength L_2). The distribution is prescribed in order to maintain a forced system.

(4) Boundary conditions at the $x = L_e$ inflow boundary are then set by assuming that uniform flow exists there (i.e. $\mathbf{U}_{i,j}^{n+1}$ is obtained for $i = NX+1$; $j = 2, \ldots, NY$).

(5) A spatial periodicity condition in the y-direction, of wavelength L_2, enables $\mathbf{U}_{i,j}^{n+1}$ to be obtained for $i = 1, \ldots, NX+1$; $j = 1$ and $i = 1, \ldots, NX+1$; $j = NY+1$.

The updating sequence can then be continued to time level $n+2$, and so on.

3. FINITE-DIFFERENCE SCHEMES AND BOUNDARY TREATMENTS

3.1. *Two-step, central-difference scheme for interior points*

An explicit, two-step, second-order accurate scheme based on the conservation form of the governing equations (1) is used. Second-order accurate operations of central-differencing and averaging are used for evaluating derivatives on the non-uniform grid (Figure 2): using full points

$$\left(\frac{df}{dx}\right)_i = a_i f_{i+1} + b_i f_i - c_i f_{i-1} \tag{4}$$

using half-points

$$\left(\frac{df}{dx}\right)_i = 2(a_i f_{i+\frac{1}{2}} + b_i f_i - c_i f_{i-\frac{1}{2}}) \tag{5}$$

where

$$a_i = \frac{\Delta x_{i-1}}{\Delta x_i(\Delta x_{i-1} + \Delta x_i)}; \qquad b_i = \frac{\Delta x_i - \Delta x_{i-1}}{\Delta x_{i-1}\Delta x_i}; \qquad c_i = \frac{\Delta x_i}{\Delta x_{i-1}(\Delta x_{i-1} + \Delta x_i)} \tag{6}$$

Equations (4) and (5) are second-order accurate and reduce to the familiar central difference forms when $\Delta x_{i-1} = \Delta x_i$.

Figure 3 shows the finite-difference cell.

Equation (1) is differenced in a manner similar to that adopted by Burstein,[4] i.e. consider satisfying (1) at point $(i, j, n+\frac{1}{2})$ so that

$$\left(\frac{\partial \mathbf{U}}{\partial t} + \frac{\partial \mathbf{F}}{\partial x} + \frac{\partial \mathbf{G}}{\partial y}\right)_{i,j}^{n+\frac{1}{2}} = 0$$

Therefore

$$\left(\frac{\partial \mathbf{U}}{\partial t}\right)_{i,j}^{n+\frac{1}{2}} = -\left(\frac{\partial \mathbf{F}}{\partial x}\right)_{i,j}^{n+\frac{1}{2}} - \left(\frac{\partial \mathbf{G}}{\partial y}\right)_{i,j}^{n+\frac{1}{2}}$$

averaging the spatial derivatives gives (to second-order accuracy)

$$\frac{\mathbf{U}_{i,j}^{n+1} - \mathbf{U}_{i,j}^{n}}{\Delta t} = -\frac{1}{2}\left[\left(\frac{\partial \mathbf{F}}{\partial x}\right)_{i,j}^{n+1} + \left(\frac{\partial \mathbf{F}}{\partial x}\right)_{i,j}^{n}\right] - \frac{1}{2}\left[\left(\frac{\partial \mathbf{G}}{\partial y}\right)_{i,j}^{n+1} + \left(\frac{\partial \mathbf{G}}{\partial y}\right)_{i,j}^{n}\right]$$

The spatial derivatives in the x-direction are differenced according to (4) and (5) and in the y-direction the usual central difference approximation for derivatives on an equally spaced grid is used—the result is

$$\mathbf{U}_{i,j}^{n+1} = \mathbf{U}_{i,j}^{n} - \Delta t\left[a_i \mathbf{F}_{i+\frac{1}{2},j}^{n+1} + b_i \mathbf{F}_{i,j}^{n+1} - c_i \mathbf{F}_{i-\frac{1}{2},i}^{n+1} + \frac{a_i \mathbf{F}_{i+1,j}^{n} + b_i \mathbf{F}_{i,j}^{n} - c_i \mathbf{F}_{i-1,j}^{n}}{2}\right]$$

$$-\frac{\Delta t}{2\Delta y}\left[\mathbf{G}_{i,j+\frac{1}{2}}^{n+1} - \mathbf{G}_{i,j-\frac{1}{2}}^{n+1} + \frac{\mathbf{G}_{i,j+1}^{n} - \mathbf{G}_{i,j-1}^{n}}{2}\right] \tag{7}$$

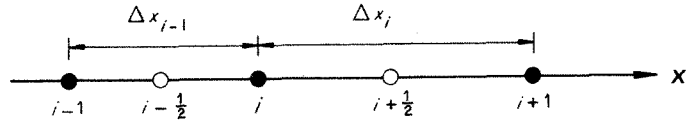

Figure 2. Grid point notation for non-uniform grid

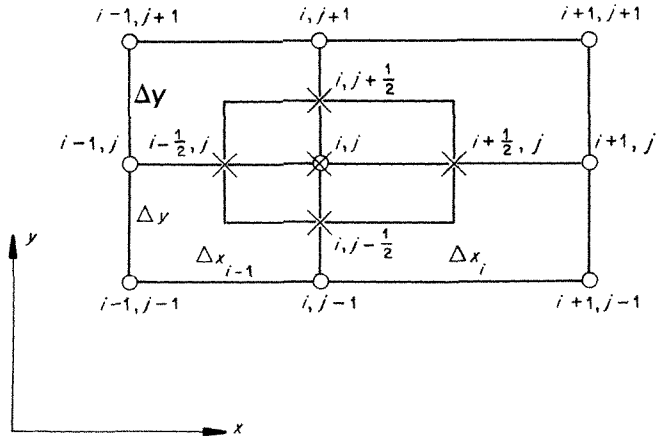

Figure 3. Finite-difference cell for two-step interior point scheme

Equation (7) is used to advance the solution at point (i, j) to time level $n+1$. To do this however, temporary values of $\mathbf{U}^{n+1}_{i\pm\frac{1}{2},j}$, $\mathbf{U}^{n+1}_{i,j\pm\frac{1}{2}}$ and $\mathbf{U}^{n+1}_{i,j}$ are required in order to evaluate the R.H.S. of (7) since $\mathbf{F}^{n+1}_{i+\frac{1}{2},j}=\mathbf{F}(\mathbf{U}^{n+1}_{i+\frac{1}{2},j})$, etc. (the location of the temporary values is denoted by $\times$ in Figure 3). Consider, therefore, satisfying equation (1) at point $(i+\frac{1}{2}, j, n)$ so that

$$\left(\frac{\partial \mathbf{U}}{\partial t}\right)^n_{i+\frac{1}{2},j}=-\left(\frac{\partial \mathbf{F}}{\partial x}\right)^n_{i+\frac{1}{2},j}-\left(\frac{\partial \mathbf{G}}{\partial y}\right)^n_{i+\frac{1}{2},j}$$

forward time differencing and central space differencing then produce an expression for $\mathbf{U}^{n+1}_{i+\frac{1}{2},j}$ (the other temporary values are obtained in a similar manner). The full set of temporary values is given by:

$$\mathbf{U}^{n+1}_{i\pm\frac{1}{2},j}=\frac{\mathbf{U}^n_{i\pm1,j}+\mathbf{U}^n_{i,j}}{2}\mp\frac{\Delta t}{\Delta x_{i\,(i-1)}}[\mathbf{F}^n_{i\pm1,j}-\mathbf{F}^n_{i,j}]-\frac{\Delta t}{\Delta y}[\mathbf{G}^n_{i\pm\frac{1}{2},j+\frac{1}{2}}-\mathbf{G}^n_{i\pm\frac{1}{2},j-\frac{1}{2}}] \tag{8}$$

$$\mathbf{U}^{n+1}_{i,j\pm\frac{1}{2}}=\frac{\mathbf{U}^n_{i,j\pm1}+\mathbf{U}^n_{i,j}}{2}-2\Delta t[a_i\mathbf{F}^n_{i+\frac{1}{2},j\pm\frac{1}{2}}+b_i\mathbf{F}^n_{i,j\pm\frac{1}{2}}-c_i\mathbf{F}^n_{i-\frac{1}{2},j\pm\frac{1}{2}}]\mp\frac{\Delta t}{\Delta y}[\mathbf{G}^n_{i,j\pm1}-\mathbf{G}^n_{i,j}] \tag{9}$$

$$\mathbf{U}^{n+1}_{i,j}=\frac{\mathbf{U}^n_{i,j+1}+2\mathbf{U}^n_{i,j}+\mathbf{U}^n_{i,j-1}}{4}-2\Delta t[a_i\mathbf{F}^n_{i+\frac{1}{2},j}+b_i\mathbf{F}^n_{i,j}-c_i\mathbf{F}^n_{i-\frac{1}{2},j}]-\frac{\Delta t}{2\Delta y}[\mathbf{G}^n_{i,j+1}-\mathbf{G}^n_{i,j-1}] \tag{10}$$

Values at points such as $(i+\frac{1}{2}, j+\frac{1}{2})$, etc., in (8) and (9) are obtained by averaging the values at surrounding grid points i.e.

$$\mathbf{F}^n_{i+\frac{1}{2},j+\frac{1}{2}}=\frac{\mathbf{F}^n_{i,j+1}+\mathbf{F}^n_{i+1,j+1}+\mathbf{F}^n_{i+1,j}+\mathbf{F}^n_{i,j}}{4} \tag{11}$$

The values of **F** at the half-points in (9) and (10) are obtained as follows:

$$\mathbf{F}^n_{i\pm\frac{1}{2},j}=\frac{\mathbf{F}^n_{i\pm1,j}+\mathbf{F}^n_{i,j}}{2}$$
$$\mathbf{F}^n_{i,j\pm\frac{1}{2}}=\frac{\mathbf{F}^n_{i,j\pm1}+\mathbf{F}^n_{i,j}}{2} \tag{12}$$

For a uniform grid (constant $\Delta x, \Delta y$) the scheme reduced to the inviscid part of a scheme used by Palumbo and Rubin[5] for viscous, blunt body flows. Also for a uniform grid, a linear stability analysis provides the following stability criterion:

$$\text{C.F.L.}=(\sqrt{(u^2+v^2)}+c)\frac{\Delta t}{\Delta_{\min}}\leq\frac{1}{\sqrt{2}} \tag{13}$$

where $\Delta_{\min}$ = minimum of Δx or Δy.

3.1.1. *Two-step, one-sided scheme for the outflow boundary.* This scheme is second-order accurate and has a similar structure to the two-step interior point scheme.

The following expressions are used to approximate the spatial derivatives (on a uniformly spaced streamwise grid, Figure 4): Derivatives at time level n

$$\left(\frac{df}{dx}\right)_i=\frac{-f_{i+2}+4f_{i+1}-3f_i}{2\Delta x} \tag{14}$$

and (for the temporary values)

$$\left(\frac{df}{dx}\right)_i=\frac{-f_{i+\frac{5}{2}}+3f_{i+\frac{3}{2}}-2f_{i+\frac{1}{2}}}{\Delta x} \tag{15}$$

Derivatives at time level $n+1$

$$\left(\frac{df}{dx}\right)_i=\frac{-3f_{i+\frac{3}{2}}+8f_{i+1}-5f_{i+\frac{1}{2}}}{\Delta x} \tag{16}$$

Equations (14)–(16) are second-order accurate. The finite-difference cell is shown in Figure 5.

The complete scheme is:

$$\mathbf{U}^{n+1}_{i,j}=\mathbf{U}^n_{i,j}-\frac{\Delta t}{2\Delta x}\left[(-3\mathbf{F}^{n+1}_{i+\frac{3}{2},j}+8\mathbf{F}^{n+1}_{i+1,j}-5\mathbf{F}^{n+1}_{i+\frac{1}{2},j})+\frac{(-\mathbf{F}^n_{i+2,j}+4\mathbf{F}^n_{i+1,j}-3\mathbf{F}^n_{i,j})}{2}\right]$$
$$-\frac{\Delta t}{2\Delta y}\left[\mathbf{G}^{n+1}_{i,j+\frac{1}{2}}-\mathbf{G}^{n+1}_{i,j-\frac{1}{2}}+\frac{\mathbf{G}^n_{i,j+1}-\mathbf{G}^n_{i,j-1}}{2}\right] \tag{17}$$

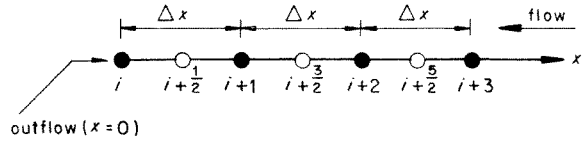

Figure 4. Grid point notation for uniform grid at outflow

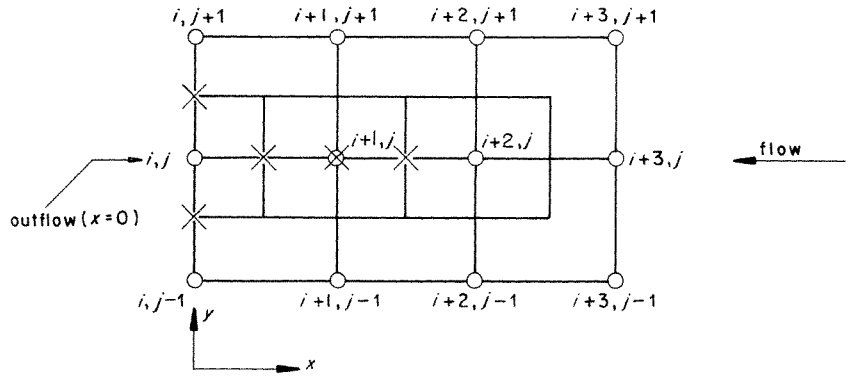

Figure 5. Finite-difference cell for two-step outflow boundary scheme

The temporary values at $\mathbf{U}^{n+1}_{i+\frac{1}{2},j}$, $\mathbf{U}^{n+1}_{i+1,j}$, $\mathbf{U}^{n+1}_{i+\frac{3}{2},j}$ needed in (17) are obtained when the interior points are updated (i.e. they are given by equations (8), (7) and (8), respectively, and need not be re-calculated). The temporary values at $\mathbf{U}^{n+1}_{i,j\pm\frac{1}{2}}$ are given by:

$$\mathbf{U}^{n+1}_{i,j\pm\frac{1}{2}} = \frac{\mathbf{U}^n_{i,j\pm1}+\mathbf{U}^n_{i,j}}{2} - \frac{\Delta t}{\Delta x}\left[-\mathbf{F}^n_{i+\frac{5}{2},j\pm\frac{1}{2}} + 3\mathbf{F}^n_{i+\frac{3}{2},j\pm\frac{1}{2}} - 2\mathbf{F}^n_{i+\frac{1}{2},j\pm\frac{1}{2}}\right]$$
$$\mp\frac{\Delta t}{\Delta y}\left[\mathbf{G}^n_{i,j\pm1} - \mathbf{G}^n_{i,j}\right] \tag{18}$$

The temporary values of $\mathbf{U}^{n+1}$ are denoted by $\times$ in Figure 5. Values such as $\mathbf{F}^n_{i+\frac{5}{2},j+\frac{1}{2}}$, etc., are obtained by averaging the values at surrounding grid points as in (11).

3.2. One-step, central-difference scheme for interior points and corresponding outflow boundary scheme

As an alternative to the two-step interior point scheme (and for comparison purposes) a simple, one-step, explicit, first-order accurate scheme is used. It is formed by forward time-differencing equation (1) to give

$$\mathbf{U}^{n+1}_{i,j} = \mathbf{U}^n_{i,j} - \Delta t\left(\frac{\partial \mathbf{F}}{\partial x}\right)^n_{i,j} - \Delta t\left(\frac{\partial \mathbf{G}}{\partial y}\right)^n_{i,j}$$

If central-differencing is used for the spatial derivatives a numerically unstable scheme results. However, if $\mathbf{U}^n_{i,j}$ is averaged, then central-differencing can be retained and the following stable scheme results:

$$\mathbf{U}^{n+1}_{i,j} = \frac{\mathbf{U}^n_{i+1,j}+\mathbf{U}^n_{i-1,j}+\mathbf{U}^n_{i,j+1}+\mathbf{U}^n_{i,j-1}}{4}$$
$$-\frac{\Delta t}{(\Delta x_{i-1}+\Delta x_i)}\left[\mathbf{F}^n_{i+1,j}-\mathbf{F}^n_{i-1,j}\right] - \frac{\Delta t}{2\Delta y}\left[\mathbf{G}^n_{i,j+1}, -\mathbf{G}^n_{i,j-1}\right] \tag{19}$$

This scheme possesses high dissipation (i.e. numerical damping, as is shown by the numerical results in Section 4), and is sometimes referred to as the Lax-Friedrichs scheme (see Reference 6, pp. 242–244). Roache[6] also gives the following linear stability criterion for (19)

on a uniform grid (constant $\Delta x, \Delta y$):

$$(\sqrt{(u^2+v^2)}+c)\frac{\Delta t}{\Delta x\,\Delta y}\sqrt{(\Delta x^2+\Delta y^2)}\leq 1 \tag{20}$$

Using one-sided differencing in the x-direction, the corresponding scheme for the outflow boundary is

$$\mathbf{U}_{i,j}^{n+1}=\mathbf{U}_{i,j}^{n}-\frac{\Delta t}{\Delta x}[\mathbf{F}_{i+1,j}^{n}-\mathbf{F}_{i,j}^{n}]-\frac{\Delta t}{2\Delta y}[\mathbf{G}_{i,j+1}^{n}-\mathbf{G}_{i,j-1}^{n}] \tag{21}$$

3.3. Setting prescribed conditions along the outflow boundary

3.3.1. *Setting the streamwise velocity distribution.* The conservation variables (ρ, m, n, e_v) are updated along the outflow boundary, to time level $n+1$. These are then converted to values of density, velocity and pressure (i.e. to (ρ, u, v, p)).

The updated streamwise velocity (u) is then replaced by a prescribed distribution (denoted u^*) on the interval $0\leq y\leq L_2$. New conservation values (denoted by m^* and e_v^*) are then formed as follows:

$$\begin{aligned} m^* &= \rho u^* \\ e_v^* &= e_v+\frac{m^{*2}-m^2}{2\rho} \end{aligned} \tag{22}$$

The conservation variables (ρ, m^*, n, e_v^*) are then used in the next stage of updating.

By forming m^* and e_v^* in this manner, only the updated values of streamwise velocity are altered (i.e. the updated values (ρ, u, v, p) are altered to (ρ, u^*, v, p) at the same time level).

3.3.2. *Setting the pressure distribution.* In this case the updated pressure (p) is replaced by a prescribed distribution (denoted p^*) on the interval $0\leq y\leq L_2$. New conservation values of energy (denoted by e_v^*) are then formed as follows:

$$e_v^*=\frac{p^*}{\gamma-1}+\frac{m^2+n^2}{2\rho} \tag{23}$$

By forming e_v^* in this manner, only the updated values of pressure are altered (i.e. the updated values (ρ, u, v, p) are altered to (ρ, u, v, p^*) at the same time level).

3.4. Inflow boundary procedure

The boundary was initially placed at $x=L_1$ (see Figure 1) and various extrapolation procedures were used to set the boundary values.

This approach was found to be unsatisfactory, either instabilities were induced or the extrapolation methods tended to become too intricate in detail, and therefore so problem-dependent, as to be of little general use. These procedures are summarized in Appendix II.2.

Owing to the inadequacies of extrapolation at $x=L_1$, the inflow boundary is placed at a large distance from outflow so that a uniform flow can be assumed at $x=L_e$.

In order to set the boundary conditions, a phenomenon of the non-linear wave propagation must first be anticipated—that of causing a change in mean values of the flow properties. Examination of the small-perturbation solution (42) shows that along any line $x=$ constant, in the interval $0\leq y\leq L_2$ (and assuming $k=2\pi/L_2$), the variations consist of the uniform stream values plus one wavelength of a sinusoidal perturbation. The means of the variations are therefore the uniform stream values (i.e. the means of the perturbations are zero). However, the numerical results presented in Section 4 show that the means differ from the

uniform stream values set initially. The means of ρ, u and p were found to change in the form of a plane wave which propagated through the medium from outflow to inflow at an approximate speed given by

$$c_s = C_0 + U_0 \tag{24}$$

which is the speed of small disturbances in the uniform stream. This wave motion forms part of the start-up transient and provision for the variation in the means must be made at the inflow boundary (as the field approaches a periodic state, the mean levels become steady and, as will be shown in the results section, mass and momentum become closely conserved in the region over a cyclic interval).

The variation of the means is governed by the equation

$$\frac{\partial M}{\partial t} + c_s \frac{\partial M}{\partial x} = 0 \tag{25}$$

where $M = M(x, t)$ is the mean of ρ, u or p along line x at time t on the interval $0 \leq y \leq L_2$. The solution of (25) is $M(x, t) = M(x - c_s t)$, which is a plane wave moving in the x-direction at speed c_s. Equation (25) is updated at inflow by the following expressions:

(i) *Uniform grid at inflow*

$$M_i^{n+1} = M_i^n - \frac{c_s \Delta t}{2\Delta x}[M_{i-2}^n - 4M_{i-1}^n + 3M_i^n] + \frac{1}{2}\left(\frac{c_s \Delta t}{\Delta x}\right)^2 [M_i^n - 2M_{i-1}^n + M_{i-2}^n] \tag{26}$$

Scheme (26) is based on the single-step Lax–Wendroff method (Reference 7, pp. 300–302). The spatial derivatives are approximated by one-sided differencing. (26) is stable if

$$c_s \frac{\Delta t}{\Delta x} \leq 2 \quad (\text{for } c_s \geq 0)$$

(ii) *Expanding grid at inflow*

$$M_i^{n+1} = M_i^n - c_s \frac{\Delta t}{h}[M_i^n - M_{i-1}^n] \tag{27}$$

which is stable if $c_s \dfrac{\Delta t}{h} \leq 1$ (assuming $c_s \geq 0$).

Uniform flow conditions at inflow are then set by the following:

$$\begin{aligned} \rho &= \rho_{\text{mean}} \\ u &= u_{\text{mean}} \\ v &= 0 \\ p &= p_{\text{mean}} \end{aligned} \tag{28}$$

where the means are given by (26) or (27) ($\mathbf{U}_{NX+1,J}^{n+1}$ is then formed from these values).

3.5. *Side boundaries*

A spatial periodicity condition in the y-direction is enforced so that the variations a distance L_2 apart will be equal. This is achieved by setting

$$\mathbf{U}_{i,1}^{n+1} = \mathbf{U}_{i,NY-1}^{n+1} \tag{29}$$

and

$$\mathbf{U}_{i,NY+1}^{n+1} = \mathbf{U}_{i,3}^{n+1} \tag{30}$$

4. RESULTS AND DISCUSSION

Figures 6(a) and 6(b) show the streamwise grids used. The expanding grid region in Figure 6(b) has $\Delta x_{i+1} = r\Delta x_i$, where $r = 1{\cdot}1$. For both grids $L_1 = 80\,\Delta x$, $L_2 = 40\,\Delta y$, with $\Delta y/\Delta x = 11/8$.

The majority of the computations were carried out using the following perfect gas constants and uniform stream values:

$$\left.\begin{aligned} c_p &= 1006\ \mathrm{Jkg^{-1}\,K^{-1}}; \qquad \gamma = 1{\cdot}4 \\ P_0 &= 10^5\ \mathrm{Nm^{-2}}; \qquad T_0 = 300\ \mathrm{K} \\ M_x &= -0{\cdot}5 \text{ (therefore } U_0 = -0{\cdot}5C_0) \end{aligned}\right\} \tag{31}$$

The computation of a spatially decaying amplitude system was undertaken (for which Solution A (42) is the small-perturbation counterpart). Solution A was used to set the initial values by defining the following;

$$\begin{aligned} k &= 2\pi/L_2 \quad (\text{for } L_2 = 0{\cdot}20955\ \mathrm{m}) \\ f &= 1368\ \mathrm{Hz} \\ A_p &= 10^4\ \mathrm{Nm^{-2}} \end{aligned}$$

Equation (43) was then used to determine the amplitudes A_u and A_v, the numerical values are:

$$\begin{aligned} A_u &= 14{\cdot}538670\ \mathrm{ms^{-1}} \\ A_v &= 22{\cdot}279470\ \mathrm{ms^{-1}} \end{aligned} \tag{32}$$

Equations (42) were then evaluated at $t = 0$ and an initial conservation vector, $\mathbf{U}$, set.

The relative Mach number of the wave in the y-direction, M_{y_r} (defined in Appendix I.2.1) is $\simeq 0{\cdot}825$, which satisfies the criterion for a non-uniform amplitude solution of (36).

Solution A was also used to prescribe the values of u or p along the outflow boundary, each time-step, in accordance with the procedures outlined in Sections 3.3.1, and 3.3.2. To

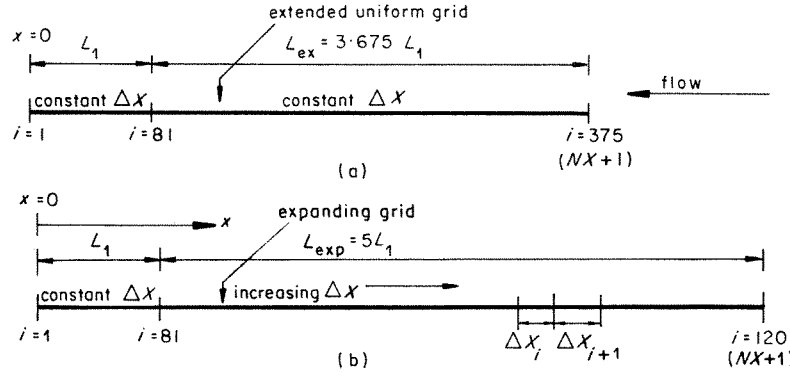

Figure 6. Streamwise grids used for computations: (a) extended uniform grid, (b) uniform-expanding grid

prescribe u, (42a) is evaluated at $x=0$; to prescribe p, (42c) is evaluated at $x=0$. The prescribed u variation is a wave of amplitude A_u, whereas the prescribed p variation is a wave of amplitude A_p (i.e. 1/10 of an 'atmosphere', P_0); the prescribed variation moves in the y-direction at a speed $c_y = C_0 M_{y_r} \simeq 286{\cdot}6\ \mathrm{ms}^{-1}$.

The time-step was set with the aid of the relation

$$\Delta t = 1/(f\,.\,NTC) \tag{33}$$

Where NTC = number of time-steps per cycle of the prescribed variation; for $NTC = 180$, maximum C.F.L. values of approximately 0·55 were obtained, thus satisfying the stability criterion (13).

As an aid to presentation, a Fourier analysis was performed on the variations. Consider, for example, the computed pressure along the line x = constant at time t (denoted p_c), a Fourier analysis enables this to be written as

$$p_c(y) = p_{\mathrm{mean}} + \sum_{r=1}^{\infty} p_{(r)} \sin\left(\frac{2\pi r y}{L_2} + \phi_{(r)}\right) \tag{34}$$

where p_{mean} is the mean of p_c on the Fourier interval $0 \leq y \leq L_2$, $p_{(r)}$ is the amplitude and $\phi_{(r)}$ the phase of the rth-order component of p_c. The corresponding small-perturbation solution given by (42c) has the form

$$p(y) = P_0 + A_x \sin\left(\frac{2\pi y}{L_2} + \alpha\right) \tag{35}$$

which may be regarded as a 'first-order' solution to the non-linear problem (i.e. comprising a mean + a single harmonic of wavelength L_2). By performing the analysis along each line, x = constant, in the grid at fixed times (after integral numbers of cycles of the prescribed variable at the outflow boundary have elapsed), the streamwise distributions of the means, amplitudes and phases of the variations were obtained.

The first calculation was performed on the extended uniform grid shown in Figure 6(a). The two-step scheme was used to update the interior points and u was prescribed along outflow as outlined in Section 3.3.1. The means of ρ, u and p were updated at inflow by using (26) for c_s given by (24) (i.e. in the case $c_s = 0{\cdot}5\ C_0$). The inflow boundary conditions were set according to (28).

Figures 7(a), (b), (c) show how the means distributions develop with time. Since the initial values consist of the uniform stream values plus one wavelength of a sinusoidal perturbation along each grid line x = constant, the means at $t=0$ (0 cycles) are $\rho_{\mathrm{mean}} = \rho_0$, $u_{\mathrm{mean}} = U_0$, $v_{\mathrm{mean}} = 0$, $p_{\mathrm{mean}} = P_0$. The prescribed u variation also has this form, therefore $u_{\mathrm{mean}} = U_0$ at the outflow boundary at all times. The means of ρ, u and p develop in the form of a plane wave which moves towards inflow at very nearly the disturbance speed c_s (as defined by (24)). The means of v develop in a different manner, as shown. After 16 cycles (i.e. after 16 wavelengths of the prescribed u variation have passed along the outflow boundary) the start-up transient has propagated out of the region to leave an almost steady distribution of mean values. Thus the passage of the large amplitude wave causes a change in the mean values set initially (this implies that the wave develops an asymmetry with respect to the original mean values).

Figures 8(a), (b), (c) show how the pressure amplitude distributions develop with time. These are obtained from the Fourier analysis and amplitude distributions of the first three pressure components are shown (the fourth and fifth-order components have peak amplitudes of the order of $1000\ \mathrm{Nm}^{-2}$, amplitudes of the higher-order components are less

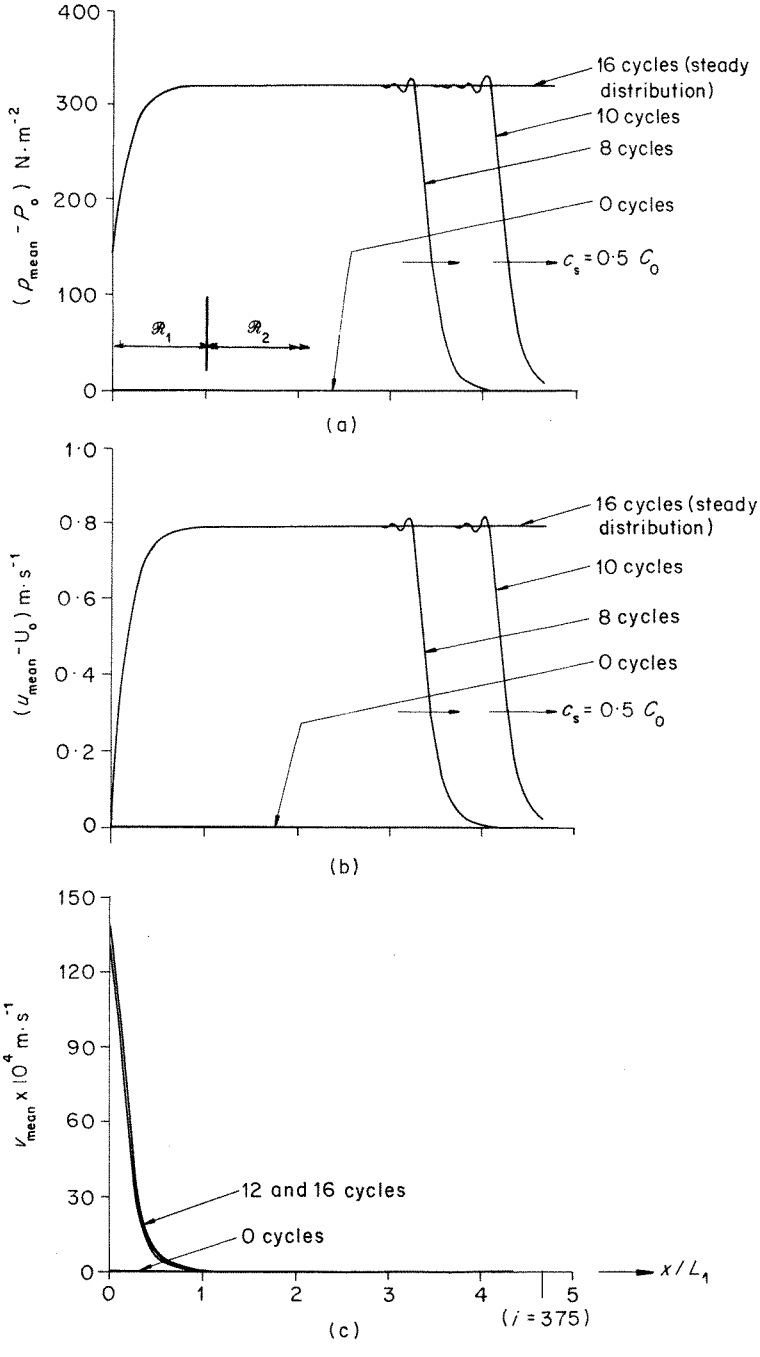

Figure 7. Variation of mean p, u, and v using two-step interior point scheme on extended uniform grid with u prescribed along outflow boundary

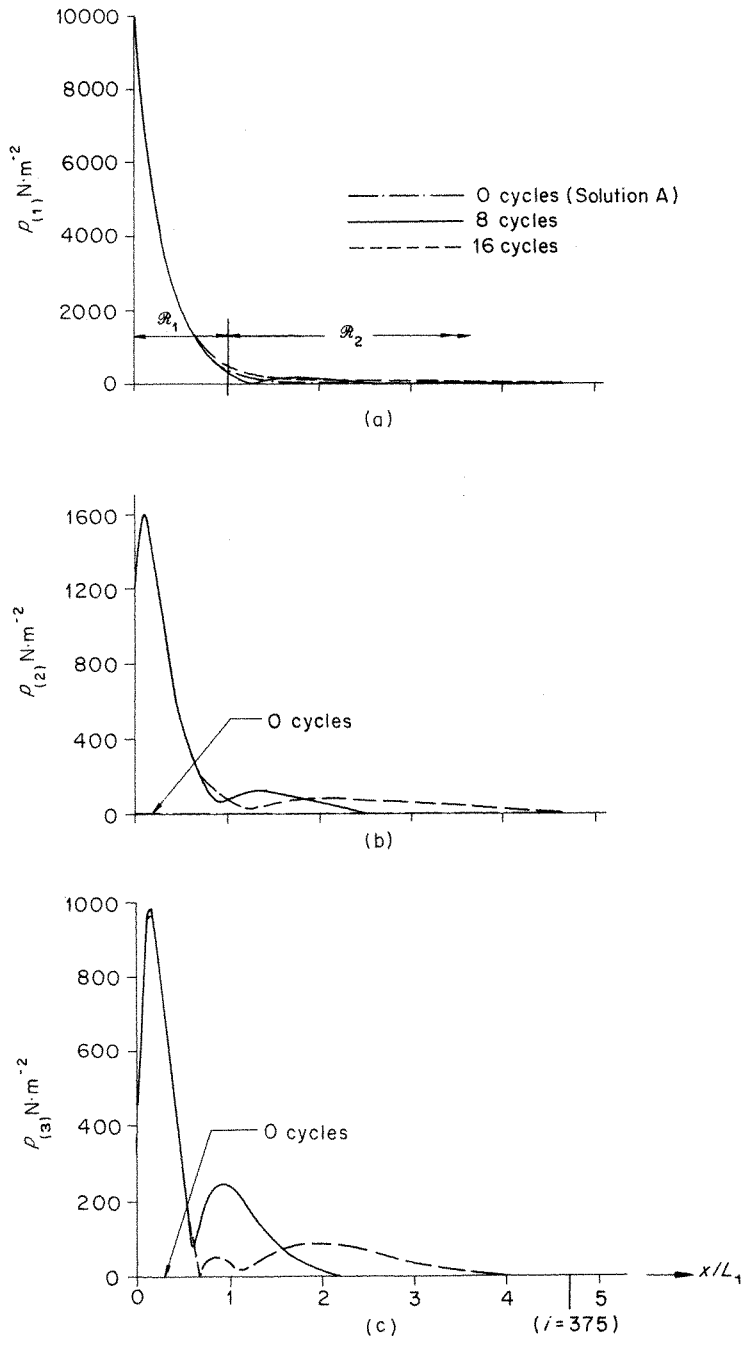

Figure 8. Variation of first, second and third-order pressure component amplitudes using two-step interior point scheme on extended uniform grid with u prescribed along outflow boundary

significant). The calculation was stopped after 16 cycles because a build-up of the first-order pressure component amplitudes was observed near the inflow boundary. Continuing the calculation beyond this stage, using the uniform inflow assumption, results in unwanted reflections propagating back into the region. The amplitudes are seen to converge towards a steady distribution (especially in the region $0 \leq x \leq L_1$). Therefore after 16 cycles the field is close to a periodic state at the frequency of the prescribed u variation. At time $t = 0$ all the component amplitudes except the first were zero. The higher-order components develop from the 'first-order' initial values as a result of non-linearities present in the governing equations. The first-order component amplitudes retain a close similarity with the exponentially decaying distribution set at $t = 0$.

Because a travelling wave solution is obtained, the amplitude distributions of the ρ, u and v components are similar in shape to the pressure amplitude distributions shown, except for slight differences near the outflow boundary. These differences occur because u has only a single component at outflow (i.e. $u_{(1)} = A_u$, $u_{(2)} = u_{(3)} = \ldots = 0$, at all times). However, since u is the only variable altered during the prescribed boundary treatment, ρ, v and p will be free to develop small higher-order components, and changes in mean values, at the outflow boundary (Figures 8(b), (c) show this effect clearly in the case of the pressure amplitudes). The amount by which u is altered in the prescribed outflow boundary treatment is very small (e.g. at 16 cycles, the difference between the updated velocity (u) and the prescribed velocity (u^*) which is used to replace it, is a maximum of $\simeq 0{\cdot}6$ per cent of the amplitude (A_u) of the prescribed velocity, i.e. $\max |u^* - u| \times 100/A_u \simeq 0{\cdot}6$). Table I shows the amplitudes and phases of the first-order components at 16 cycles at the outflow boundary for prescribed u (and p), the corresponding values given by Solution A are also given for comparison purposes.

At 16 cycles the phase distributions of the first-order components in the interval $0 \leq x \leq L_1$ are almost linear and of a similar slope to the distribution given by Solution A.

At 16 cycles, the means throughout the region and the amplitudes at the outflow boundary, are very nearly steady; near the inflow boundary the components have small amplitudes and the means of v are zero: under these conditions an examination of the mass and momentum conservation in the region was made. Since the side boundaries are spatially periodic, the net flux of mass and momentum into the region across these boundaries is zero at any instant—thus only the inflow and outflow boundaries need to be considered.

The mass and momentum transport across the inflow and outflow boundaries during one cycle were calculated as follows: at inflow, where the wave amplitudes are negligible, the mass and momentum fluxes were evaluated from the mean levels; at outflow, where the first-order components have large amplitudes, the mass and momentum fluxes were evaluated from the means and first-order components of the variations, and integrated over

Table I. Amplitudes and phases. Values at 16 cycles at $x = 0$ (outflow)

Variable	Solution A			Time-marched first-order component			
				Prescribed u		Prescribed p	
	Amplitude		Phase°	Amplitude	Phase°	Amplitude	Phase°
ρ	0·082836	kgm^{-3}	9·070	0·081549	11·422	0·082928	9·032
u	14·538670	ms^{-1}	32·559	14·538670	32·559	14·521890	29·832
v	22·279470	ms^{-1}	0·0	21·572240	2·817	22·051387	0·907
p	10000·0	Nm^{-2}	9·070	9844·7	11·317	10000·0	9·070

the cycle along the length (L_2) of the boundary. The following values were obtained:

$$m_I = 201{\cdot}009\, L_2 t_p; \qquad \dot{m}_0 = 201{\cdot}005\, L_2 t_p \text{ kg}$$
$$M_I = 135081\, L_2 t_p; \qquad M_0 = 135081\, L_2 t_p \text{ kg.m.s}^{-1}$$
$$N_I = 0; \qquad N_0 = -4{\cdot}08\, L_2 t_p \text{ kg.m.s}^{-1}$$

Therefore mass and momentum are closely conserved in the computational region over one cycle of the periodic state. A significant discrepancy in mass and momentum conservation in the region would prevent the convergence of mean levels (and amplitudes) to steady distributions.

The second calculation involved prescribing p along the outflow boundary instead of u. Thus, at outflow, $p_{\text{mean}} = P_0$, $p_{(1)} = A_p$, $p_{(2)} = p_{(3)} = \ldots, = 0$, at all times. In this case p is the only variable altered in the prescribed boundary treatment (see Section 3.3.2), therefore ρ, u and v are free to develop small higher-order components and changes in their mean values at the outflow boundary. Except in the region close to outflow, the amplitude distributions at 16 cycles were not markedly different from those obtained when u was prescribed. Figure 9(b) shows the amplitude distribution of the second-order pressure components for the two

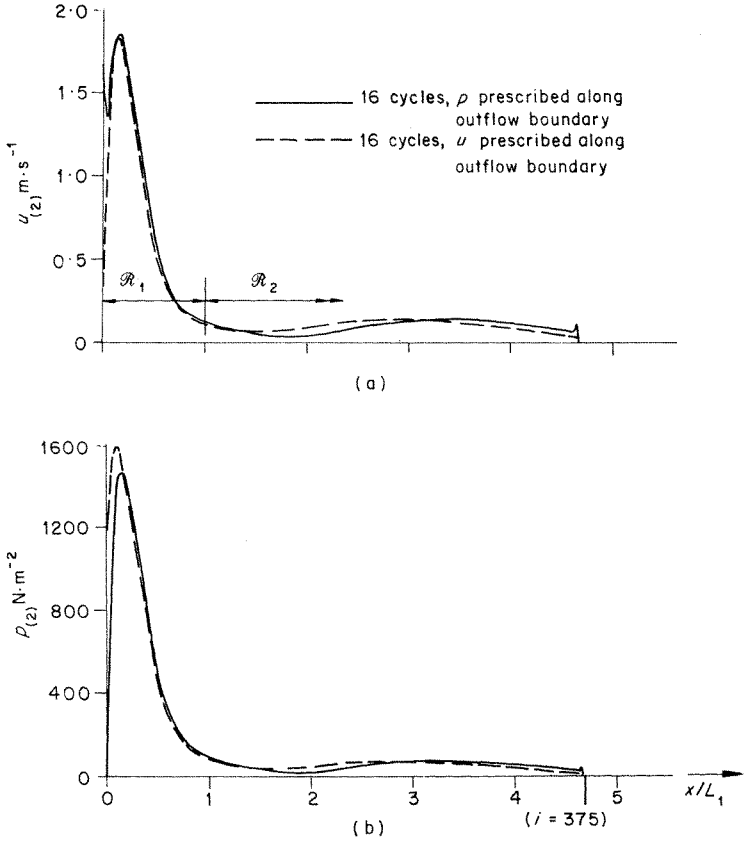

Figure 9. Second-order streamwise velocity and pressure component amplitudes at 16 cycles produced by two-step interior point scheme on extended uniform grid; difference between prescribing u or p along outflow boundary

cases. Prescribing u resulted in marginally better convergence, i.e. after 16 cycles the calculation was closer to a periodic state than was the calculation using prescribed p. However at 16 cycles, the prescribed p calculation was close enough to a periodic state to enable an examination of the mass and momentum conservation in the region to be carried out in the manner described above; mass and momentum were again found to be closely conserved in the region. The amplitudes and phases of the first-order components at 16 cycles at the outflow boundary are included in Table I.

The only significant inconsistency in the outflow boundary treatment occurs in the amplitude distribution of the second-order u component when p is prescribed at outflow. Figure 9(a) shows a sharp jump in the distribution near the outflow boundary when p is prescribed; removed from this region there is little difference between the distributions.

Various combinations of the two-step and one-step interior point schemes were used for calculations on the grid system shown in Figure 6(b) (i.e. using a uniform grid for $0 \leq x \leq L_1$ and an expanding grid for $x \geq L_1$). In these calculations u was prescribed along outflow and the means at inflow were updated using (27). The calculations were continued for 36 cycles without any evidence of instability. At inflow the amplitudes were damped to negligible values as a consequence of the expanding grid, and boundary conditions (28) could be used at all times. Figure 10 shows the resulting amplitude distributions of the first-order pressure components at 16 cycles. The damping effect of the expanding grid as well as the high inherent damping of the one-step interior point scheme are apparent from the distributions.

Figure 11 shows the development of the pressure means when the two-step scheme was used on the uniform grid with the one-step scheme on the expanding grid region. After about 6 cycles the distribution in the region $0 \leq x \leq L_1$ is almost steady, at subsequent times, outside this region, the distribution levels towards an ultimate constant value shown dotted. This levelling out occurs more rapidly (after about 30 cycles), though less smoothly, when the two-step scheme is used on both regions.

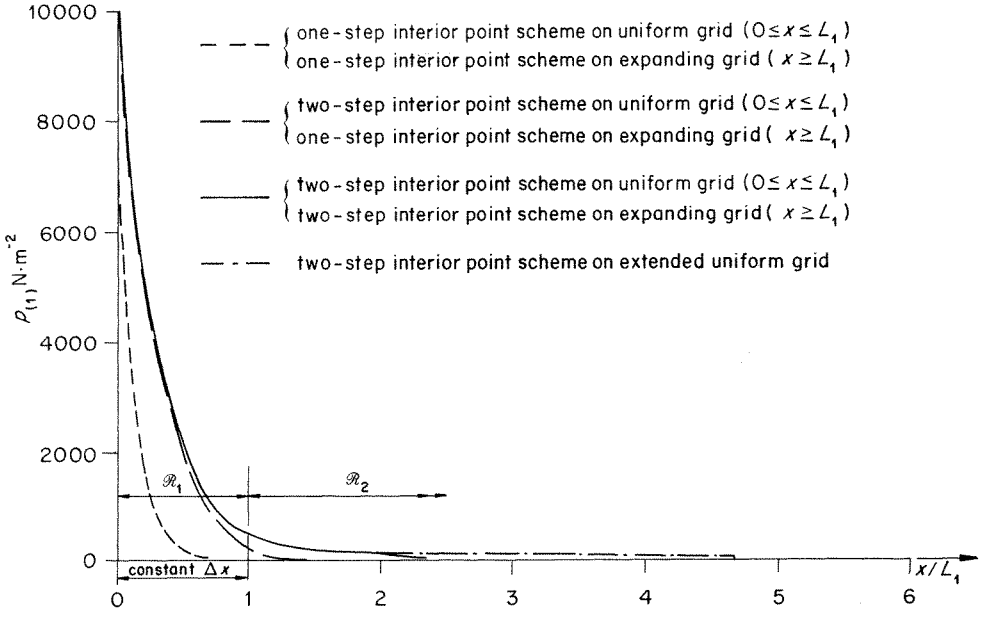

Figure 10. Comparison between first-order pressure component amplitudes at 16 cycles on extended uniform grid and on uniform-expanding grid; u prescribed along outflow boundary

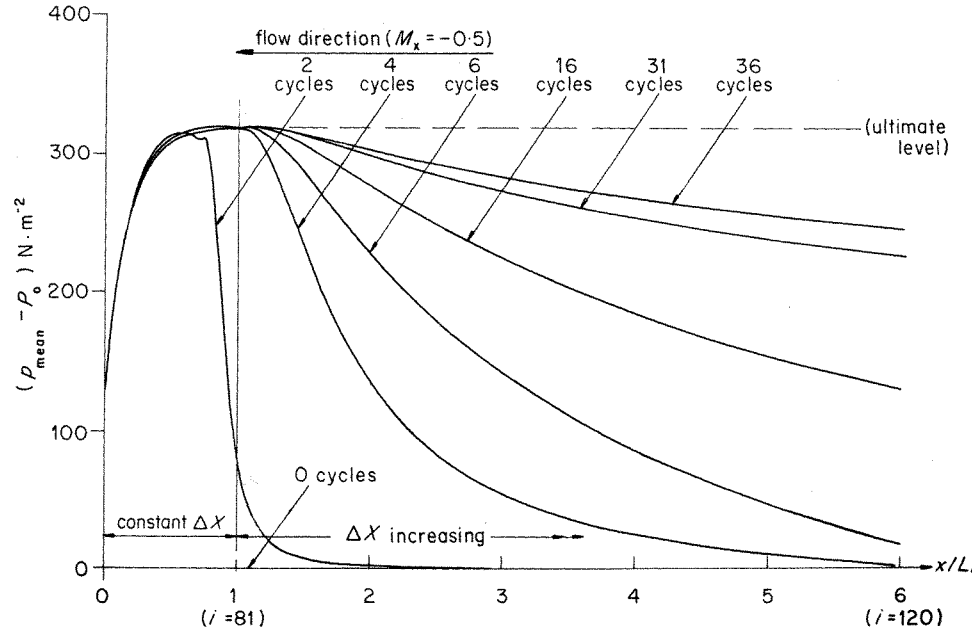

Figure 11. Variation of mean pressures produced by two-step interior point scheme on uniform grid ($0 \leq x \leq L_1$) and one-step interior point scheme on expanding grid ($x \geq L_1$); u prescribed along outflow boundary

For comparison purposes, $0 \leq x \leq L_1$ is taken to be the region where the solution is desired; the solution obtained using the extended uniform grid is used as the basis for comparisons in this region. On this basis, the solution obtained using the two-step scheme on both the uniform and expanding grid regions, is the most accurate. Examination of the distributions given by this solution at 16 and 36 cycles showed that little change occurred after 16 cycles in the region concerned. The solution obtained using the two-step scheme on the uniform grid and the one-step scheme on the expanding grid is also quite accurate. However convergence to a periodic state was slower in this case (requiring about 20 cycles for the component amplitudes to steady). The solution obtained using the one-step scheme on both the uniform and expanding grid regions has heavily damped amplitude distributions which converged after about 4 cycles; amplitudes of components greater than the second-order are negligible—this magnitude of damping is undesirable.

Table II shows a comparison of computer run times (calculations performed on a C.D.C. 7600 computer).

Table II. Computer run times

Grid system	Uniform grid scheme	Expanding grid scheme	Cycles	Time steps	Run time (s)	Cycles	Time steps	Run time (s)
Extended uniform grid Figure 6(a)	Two-step	—	16	2880	3400	—	—	—
Uniform-expanding grid Figure 6(b)	Two-step	Two-step	16	2880	1500	36	6480	3375
	Two-step	One-step	16	2880	840	36	6480	1890
	One-step	One-step	16	2880	700	36	6480	1575

Thus the use of the expanding grid, in conjunction with the two-step scheme throughout, enables an accurate solution to be obtained in the uniform grid region, $0 \leq x \leq L_1$, for less than half of the computational effort required by the extended uniform grid calculation (comparing run times for 16 cycles). The coding used for the extended uniform grid calculation was reasonably efficient: however, in the programs used for the uniform-expanding grid calculations there is much scope for improving the efficiency of the coding—the run times quoted for these cases could therefore be significantly reduced.

Further calculations of spatially decaying systems were performed for throughflow Mach numbers of $M_x = -0{\cdot}2$ and $-0{\cdot}8$ with other values as defined by relations (31) and Table III. The uniform-expanding grid of Figure 6(b) was used in conjunction with the two-step scheme throughout, u was prescribed along outflow.

Table III. Parameter values for $M_x = -0{\cdot}2$ and $-0{\cdot}8$ calculations

M_x	f(Hz)	M_{yr}	A_p (Nm^{-2})	A_u (ms^{-1})	A_v (ms^{-1})	*NTC*	C.F.L.
$-0{\cdot}2$	1525	0·920	10^4	$\simeq 10{\cdot}35$	$\simeq 25{\cdot}83$	120	$\simeq 0{\cdot}6$
$-0{\cdot}8$	950	0·573	10^4	$\simeq 20{\cdot}67$	$\simeq 15{\cdot}13$	268	$\simeq 0{\cdot}65$

The computations were run for 36 cycles and an approximate periodic state was attained in the uniform grid region $0 \leq x \leq L_1$ in about 20 cycles for $M_x = -0{\cdot}2$ and 27 cycles for $M_x = -0{\cdot}8$.

5. SUMMARY OF CONCLUSIONS

The propagation of spatially decaying finite-amplitude waves in an inviscid, perfect gas medium, was examined by time-marching methods based on finite-differences.

Numerically stable solutions were obtained by prescribing a propagating distribution of streamwise velocity or pressure along the outflow boundary. The prescribed pressure distribution had an amplitude of $10^4\,Nm^{-2}$ (equivalent to $\frac{1}{10}$ of an atmosphere). The unprescribed variables at outflow were updated by one-sided finite-difference schemes.

Conditions approaching periodic states were obtained for a wide range of subsonic throughflow Mach numbers. Non-linearity of the physical system caused higher-order components to develop from an initial single component perturbation, changes in the mean values of the initial uniform stream also occurred.

Prescribing the streamwise velocity component along outflow was found to be slightly more satisfactory than prescribing the pressure as far as convergence and physical consistency were concerned.

Two spatially centred schemes were used to update the interior points—these being a second-order accurate, two-step Lax–Wendroff method and the simple, first-order accurate, one-step Lax–Friedrichs method. Steady amplitude distributions were obtained after about 4 cycles (of the prescribed variation along outflow) when the one-step method was used. However the amplitude distributions were heavily damped as a result of high numerical dissipation in the scheme. Satisfactory amplitude distributions were obtained by using the two-step Lax–Wendroff method, though runs in excess of 16 cycles were required before an approximate periodic state was attained.

In the absence of any prescribed variation along outflow, the one-sided schemes were found to be numerically unstable when applied at a subsonic outflow boundary.

Extrapolation at the inflow boundary was found to be unsatisfactory, either gross instabilities were induced, or a general lack of convergence to temporal periodicity resulted.

Difficulties in setting the inflow boundary conditions were alleviated by using an expanding streamwise grid to follow on from a uniform grid region. This enabled the inflow boundary to be placed at a position where amplitudes had decayed to negligible values—a uniform inflow condition could then be used. The increased numerical damping in the expanding grid region did not adversely affect the variations in the uniform grid region when the two-step, Lax–Wendroff method was used to update both regions.

APPENDIX I. SMALL-PERTURBATION SOLUTIONS

The analytical, small-perturbation solution of the non-linear wave motion computed in Section 4 is given in this Appendix. The analytical solution is used to obtain initial values for the time-marching calculations, and is also used for comparison purposes.

The system of small-perturbation equations is given in Appendix I.1. A solution of the system for non-uniform amplitude waves is given in Appendix I.2. The particular solution used for setting initial values is given in Appendix I.3. This solution (referred to as Solution A) is the small-perturbation counterpart of the computed non-linear wave motion discussed in Section 4.

I.1. *Small-perturbation equations*

The small-perturbation equations are obtained by linearizing the normal (non-conservation form) Euler equations. The equation of continuity, the two equations of motion, the homentropic flow relation (i.e. $p/\rho^{\gamma} = \text{constant}$), and the equation of state, are linearized by assuming that the flow field consists of a steady uniform stream plus a small, unsteady perturbation (i.e. $u(x, y, t) = U_0 + u'(x, y, t)$, $v(x, y, t) = V_0 + v'(x, y, t)$, $p(x, y, t) = P_0 + p'(x, y, t)$, etc.; products and powers of the perturbation variables are assumed to be negligibly small quantities). The above assumption, together with that of flow irrotationality, enables the following convective wave equation in the perturbation velocity potential to be derived (where $V_0 = 0$ has been assumed):

$$\frac{\partial^2 \phi'}{\partial t^2} = C_0^2 \left[(1 - M_x^2) \frac{\partial^2 \phi'}{\partial x^2} + \frac{\partial^2 \phi'}{\partial y^2} \right] - 2U_0 \frac{\partial^2 \phi'}{\partial x \partial t} \tag{36}$$

For a prescribed uniform stream, (36) can be solved for ϕ'; the following expressions can then be used to determine the small-perturbation field:

$$\left.\begin{aligned} u' &= \frac{\partial \phi'}{\partial x}, \qquad v' = \frac{\partial \phi'}{\partial y} \\ p' &= -\rho_0 \left(\frac{\partial \phi'}{\partial t} + U_0 u' \right) \\ \rho' &= p'/C_0^2 \end{aligned}\right\} \tag{37}$$

I.2. *Solution of the convective wave equation*

For circular frequency ω and wave index k (and assuming $\omega > 0$, $k > 0$, $|M_x| < 1$), (36) has solutions of the form

$$\phi' = A e^{(\lambda i \pm \sqrt{s})x} e^{i(ky + \omega t)}; \qquad (i = \sqrt{-1}) \tag{38}$$

where A is arbitrary, and

$$\lambda = \frac{\omega M_x}{C_0 Z_x}; \qquad s = \frac{C_0^2 k^2 Z_x - \omega^2}{C_0^2 Z_x^2} \tag{39}$$

The nature of solutions (38) depends on the sign of s. For $s > 0$ a non-uniform amplitude results, for $s \leq 0$ a constant amplitude results. Furthermore, the real and imaginary parts of (38) are also solutions of (36).

I.2.1. *Non-uniform amplitude solutions.* It follows from (39) that $s > 0$ if

$$\omega < C_0 k \sqrt{Z_x} \tag{40}$$

The following non-uniform amplitude solutions of (36) can be deduced from (38):

$$\phi' = A e^{\pm x\sqrt{s}} \begin{Bmatrix} \sin \\ \cos \end{Bmatrix} (\lambda x \pm ky + \omega t) \tag{41}$$

(eight expressions). The travelling wave nature of (41) is made apparent by writing

$$\sin(\lambda x - ky + \omega t) = \sin L\left(\frac{\mathbf{L}}{L} \cdot \mathbf{r} + \frac{\omega t}{L}\right)$$

(where $\mathbf{L} = \lambda \mathbf{i} - k\mathbf{j}$ and $L^2 = \lambda^2 + k^2$), which represents a two-dimensional sinusoidal profile travelling in the $-\mathbf{L}$ direction with absolute speed $c_w = \omega/L$. This is shown geometrically in Figure 12 (where $M_x < 0$ has been assumed).

Along $x =$ constant, (41) reduces to $\phi' = B \sin(\pm ky + \omega t + \beta)$, which is a wave travelling in the $\mp y$-direction with absolute speed $c_y = \omega/k$ and amplitude B. The relative Mach number of the wave in the y-direction is defined as $M_{y_r} = \omega/kC_0$. By virtue of inequality (40) it follows that non-uniform amplitude solutions of (36) occur if $M_{y_r} < \sqrt{Z_x}$.

I.3. *Solution A*

The following non-uniform amplitude solution of (36), which has the form of (41), was used to set the initial values and the prescribed boundary conditions at outflow in the time-marching calculations discussed in Section 4:

$$\phi' = -A e^{-x\sqrt{s}} \cos(\lambda x - ky + \omega t)$$

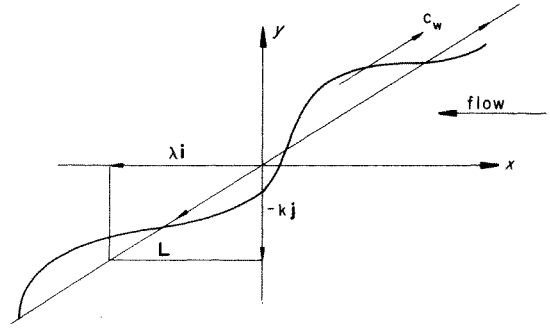

Figure 12. Two dimensional travelling wave

Equations (37) give the small-perturbation field:

$$\left.\begin{aligned} u &= U_0 + A_u e^{-x\sqrt{s}} \sin[ky - \lambda x - \omega t - \arctan(\sqrt{s}/\lambda) + \pi] \\ v &= A_v e^{-x\sqrt{s}} \sin[ky - \lambda x - \omega t] \\ p &= P_0 + A_p e^{-x\sqrt{s}} \sin[ky - \lambda x - \omega t - \arctan(U_0\sqrt{s}/(\omega + U_0\lambda))] \end{aligned}\right\} \quad (42a,b,c)$$

where

$$\left.\begin{aligned} A_u &= A\sqrt{(\lambda^2 + s)} \\ A_v &= kA \\ A_p &= \rho_0 A\sqrt{[(\omega + U_0\lambda)^2 + U_0^2 s]} \end{aligned}\right\} \quad (43)$$

and A is arbitrary. (42) is referred to as Solution A in the text.

At fixed time ($t = t_1$) along the equally spaced lines $x - \Delta x$, x, $x + \Delta x$, p' has the form

$$\left.\begin{aligned} p'(x - \Delta x, y, t_1) &= A_{x-\Delta x} \sin(ky + \varepsilon_{x-\Delta x}) \\ p'(x, y, t_1) &= A_x \sin(ky + \varepsilon_x) \\ p'(x + \Delta x, y, t_1) &= A_{x+\Delta x} \sin(ky + \varepsilon_{x+\Delta x}) \end{aligned}\right\} \quad (44)$$

where A_x is the amplitude and ε_x the phase of the variation along the line $x = $ constant, i.e.

$$\left.\begin{aligned} A_x &= A_p e^{-x\sqrt{s}} \\ \varepsilon_x &= -\lambda x + \theta \end{aligned}\right\} \quad (45)$$

where θ is a constant. Therefore at any instant the amplitudes vary exponentially, and the phases vary linearly with x (this also applies to the other perturbation variables).

APPENDIX II. SUMMARY OF BOUNDARY TREATMENTS WHICH WERE EXAMINED AND FOUND TO BE UNSATISFACTORY

II.1. *Outflow Boundary* (*at* $x = 0$, *see Figure 1*)

(a) Using the small-perturbation solution (Appendix I.3) to prescribe ρ, u, v, p at each time step.

This amounts to overprescription and generates non-physical, short wavelength disturbances.

(b) Updating all the variables by one-sided differencing after imposing an initial disturbance (the converse of (a)).

This is numerically unstable, Warming and Beam[8] use a linear stability analysis to show that it is stable in a supersonic flow and unstable in subsonic flow.

II.2. *Inflow Boundary* (*at* $x = L_1$, *see Figure 1*)

(a), Updating by one-sided differencing. A linear stability analysis shows this to be unconditionally unstable.

(b), Extrapolation of the primary variables (ρ, m, n, e_v). Three methods of extrapolation were considered:

(i) Polynomial extrapolation along $y = $ constant lines

(ii) Extrapolation using a quadratic least squares fit along $y = $ constant lines.

(iii) Extrapolation of amplitudes and phases of each component of the y-direction variations in accordance with the properties of the small-perturbation solution (i.e. an extrapolation procedure based on equation (45)).

All three methods proved to be unstable, the rate at which instability develops increasing as the number of data points used is increased. The instability is associated with the transients which reach the boundary before a periodic state is reached.

NOTATION

A = constant

A_p, A_u, A_v = peak amplitudes of p, u, v

A_x, ε_x = amplitude and phase of variation in y-direction

C.F.L. = Courant–Friedrichs–Lewy stability criterion

$c = \sqrt{(\gamma RT)}$ = 'speed of sound'

$C_0 = \sqrt{(\gamma R T_0)}$

$c_s = C_0 \pm U_0$

c_v = specific heat at constant volume

c_w = wave speed in direction of propagation

c_y = wave speed in y-direction

$e_v = \rho\left(c_v T + \dfrac{u^2+v^2}{2}\right)$ = total energy per unit volume

$\mathbf{F}, \mathbf{G}$ = vector functions of $\mathbf{U}$

$\mathbf{F}^n_{i,j}$, etc. = $\mathbf{F}$ at discrete co-ordinates (i, j, n)

f = frequency or function of x

h = streamwise grid spacing

$\mathbf{i}, \mathbf{j}$ = unit vectors in x and y directions

$\mathbf{L}$ = vector in direction of wave propagation

L = magnitude of $\mathbf{L}$

L_1, L_2 = spatial field lengths in x and y-directions

L_e, L_{ex}, L_{exp} = spatial grid lengths in x-direction (see Figs. 1, 6)

M = function representing distribution of mean quantities (see equation. (25)

M_I, M_0 = x-momentum transport across inflow and outflow boundaries during one cycle

$M_x = U_0/C_0$

$m = \rho u$ = x-momentum per unit volume

mean (subscript) = mean of variation on interval $0 \leq y \leq L_2$

m_I, m_0 = mass transport across inflow and outflow boundaries during one cycle

NTC = number of time-steps per cycle of variation

NX, NY = grid point numbers (see Figure 1)

N_I, N_0 = y-momentum transport across inflow and outflow boundaries during one cycle

$n = \rho v$ = y-momentum per unit volume

0 (subscript) = steady uniform stream values

p = pressure

p', etc = perturbation pressure

$p_{(r)}, \phi_{(r)}$ = amplitude and phase of rth-order component of p

$\mathcal{R}$ = spatial region (see Figure 1)

R = gas constant

$\mathbf{r} = x\mathbf{i} + y\mathbf{j}$ = position vector

$r = \Delta x_{i+1}/\Delta x_i$ = expanding grid ratio (see Figure 6(b)).
(r) (subscript) = component number
s = as defined by equation (39)
T = temperature
$t_p = 1/f$ = periodic time
$\mathbf{U} = (\rho, m, n, e_v)$
u = velocity in x-direction (streamwise)
$u_{(r)}$ = amplitude of rth-order component of u
v = velocity in y-direction
$Z_x = 1 - M_x^2$
α, β, θ = constants
γ = adiabatic index
λ = as defined by equation (39)
ρ = density
ϕ' = perturbation velocity potential
$\omega = 2\pi f$ = circular frequency

REFERENCES

1. R. H. Ni and F. Sisto, 'Numerical computation of non-stationary aerodynamics of flat plate cascades in compressible flow', *A.S.M.E. Journal of Engineering for Power*, **98,** 165–170 (1976).
2. G. Moretti, 'The choice of a time-dependent technique in gas dynamics', *A.G.A.R.D. Lecture Series No. 48*, 11-1, 11-28 (1971).
3. J. I. Erdos, E. Alzner and W. McNally, 'Numerical solution of periodic transonic flow through a fan stage', *A.I.A.A. Journal*, **15,** 1559–1568 (1977).
4. S. Z. Burstein, 'Finite-difference calculations for hydrodynamic flows containing discontinuities', *J. Computational Phys.*, **2,** 198–222 (1967).
5. D. J. Palumbo and E. L. Rubin, 'Solutions of the two-dimensional, unsteady, compressible Navier–Stokes equations using a second-order accurate numerical scheme', *J. Computational Phys.*, **9,** 466–495 (1972).
6. P. J. Roache, *Computational fluid dynamics*, Hermosa, Albuquerque, N.M., 1972.
7. R. D. Richtmyer and K. W. Morton, *Difference Methods for Initial-value Problems*, 2nd edn., Wiley (Interscience), New York, 1967.
8. R. F. Warming and R. M. Beam, 'Upwind second-order difference schemes and applications in aerodynamic flows', *A.I.A.A. Journal*, **14,** 1241–1249 (1976).